Short Beam Three Point Bend Tests in Syntactic Foams. Part I: Microscopic Characterization of the Failure Zones

Kishore,[1] Ravi Shankar,[2] S. Sankaran[3]

[1]*Polymer Composites Laboratory, Department of Metallurgy, Centre for Advanced Studies, Indian Institute of Science, Bangalore-560 012, India*
[2]*Department of Material Science and Engineering, North Carolina State University, Raleigh, North Carolina 27695-7907*
[3]*Aeronautical Development Establishment, C. V. Raman Nagar, Bangalore-560 093, India*

Received 20 November 2003; accepted 10 January 2005
DOI 10.1002/app.22096
Published online in Wiley InterScience (www.interscience.wiley.com).

ABSTRACT: Scanning Electron Microscopic (SEM) studies were carried out on the failure surface of syntactic foam material tested in a short beam three point bend test (SBT) by employing 21 × 15 × 3 mm^3 dimension bearing specimens. The syntactic foams were fabricated using glass microballoons in epoxy binder. The failure of the tensile, compression, and shear dominated regions were studied by SEM at different magnifications. The tensile region had characteristic features, such as partial debonding of the microballoons from the matrix and cracking of glass microballoons, apart from matrix cracking and some river pattern features. The compression side was characterized by crushing and collapsing of microballoons, resulting in accumulation of debris with no apparent river pattern for matrix-rich regions. The midway positions of the SBT failed surface comprised of deformation bands in the matrix and occasional debonding of microballoons. The morphology recorded in the tensile and compression regions corroborated well with the results obtained on these foam samples in those specimens that were subjected to pure uniaxial tension and compression, respectively. © 2005 Wiley Periodicals, Inc. J Appl Polym Sci 98: 673–679, 2005

Key words: failure zones; short beam bend test; syntactic foam and microscopy

INTRODUCTION

Syntactic foams are formed by embedding hollow microspheres, called microballoons, in polymer binder. Usually the glass microballoons embedded in syntactic foams have density in the range of 300 to 870 kg/m^3, depending upon the application. Structurally, these newer materials are categorized either as two-phase or three-phase.[1] Two-phase syntactic foams are formed by embedding glass microspheres in binder, with negligible levels of voids in the final structure, whereas the three-phase syntactic foams have a significant amount of voids trapped in as the third phase. Syntactic foams are regarded as useful and attractive materials as they have a wide range of mechanical properties coupled with vibration damping characteristics[2] and useful dielectric characteristics. They are used as core materials in composite sandwich structures for weight-sensitive structure applications where the so called "antiplane"[3] sandwich is obtained and where the roles of the core are to transmit shear stress between the skins and then to keep the skins separate by nearly a constant distance during the deformation.[3] The other advantages of these materials include the higher bending stiffness and specific strengths achievable within them.[4] The closed cell structure of these foams results in low moisture absorption and high compressive strength as compared to the conventionally used core materials, such as open cell foams and honeycomb structures.[5] Syntactic foams find major applications in aircraft and in structural components of submarines and spacecrafts.

The published literature on syntactic foams includes both experimental and theoretical aspects of characterization of foams[6,7] and their sandwich structure.[8] There are also reports of characterizing the aqueous media absorption in these systems, since they find application as buoyancy-aid material.[9] Hygrothermal response and evaluation of the residual strengths following aqueous media ingression are also studied.[10,11] Other works focus on the effect of wall thickness and radius ratio parameter of microspheres on the compressive properties of the syntactic foams.[12,13]

The available literature until now were related to the evaluation of key mechanical properties, like compressive,[14] impact[15] and flexural,[16] where it has been established that these materials have better mechanical properties, that is, higher specific strength over other traditionally made polymeric materials with

Correspondence to: Kishore (balkis@met.iisc.ernet.in).

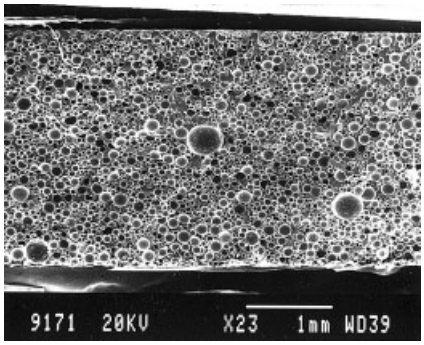

Figure 1 Low magnification macro picture showing both tension and compressive forces prevailing ends in the top and bottom part of the micrograph, respectively.

conventional fillers, such as additive,[17] oxides,[18,19] and minerals.[20,21] In all these efforts,[17–21] the focus is on determining the mechanical property data, while fracture features[22] have received lower priority. The work reported here, therefore, lays stress on studying fracture surface features of syntactic foam specimens subjected to short beam three point bend tests. This is an area where literature is scarce, compared to fiber bearing polymer systems, where a reasonably good data base exists.[19,23,24] This inadequacy of reports correlating failure features to test methods is all the more true with short beam tests, where only sporadic reports[25,26] can be found. Even in these efforts, no attempts are made to specifically characterize the fracture surface features to the dominant stress state prevailing in short beam tests, where the specimens experience compressive forces at the central point of the loading face, while the face on the opposite side experiences tensile forces. Hence, this test condition offers an ideal situation to capture the features that can record the details first on the tensile bearing surface and then move on to the compressive bearing side through a zone where shear conditions prevail. Hence, the microscopic examination should typically reveal, first, the dominance of one type each of the two stress states

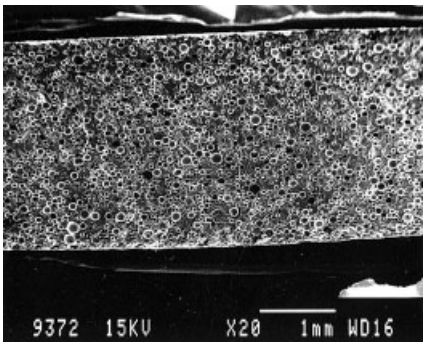

Figure 2 The arrangement in another sample, where the top is now compressive stress and the bottom is tensile stress bearing region.

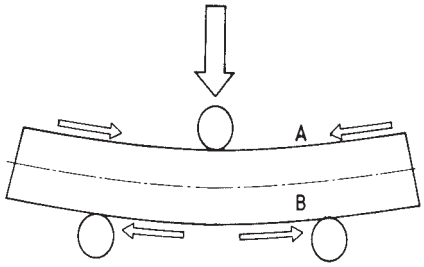

Figure 3 Schematic representation of the three point loading arrangement and the stresses prevailing on the faces A and B, respectively.

followed by a third type that lies in between. Therefore, in this work the microscopic aspects of the different zones of a short beam tested sample under three point loading are first captured as no such gradation recording on polymeric systems, whether belonging to syntactic foams or other types, could be traced from a search of reported literature. This fractographic study was followed by a comparison with those microscopic features obtained on the very same materials subjected to pure uniaxial tensile or compressive loading conditions. Thus, the work addresses for the first time the failure features in short beam tested (SBT) and failed samples across their separated cross section and then reports the comparative failure features obtained on specimens independently subjected to pure uniaxial tension (UT) and compression (UC) in the similarly made syntactic foam (SF) material.

EXPERIMENTAL

Materials

An epoxy system consisting of Araldite LY-556 (Bisphenol -A Diglycidyl ether) and Hardener HT-972 (aromatic diamine) supplied by Vantico Performance Polymers Pvt. Ltd. is employed. The value of EEW of this resin, as specified by the manufacturer, is 190. Resin and hardener were mixed in 100 : 27 ratio by weight. The density of the cured resin system was

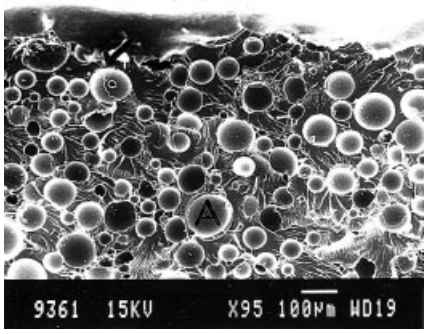

Figure 4 Tension bearing region where the top part shows the crack initiation process (shown by an arrow).

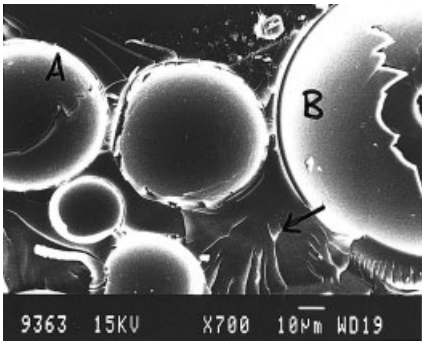

Figure 5 Central microballoon displaying interface debonding in the top left. Also visible is the equatorial crack on the left top corner as well as the right top corner positioned microballoons.

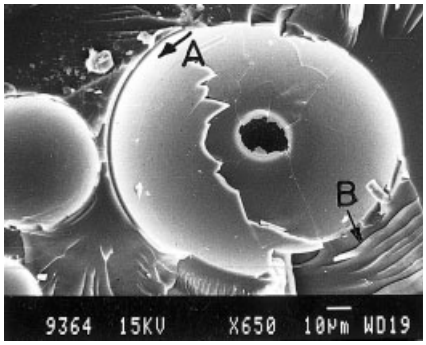

Figure 7 The features of interface debonding between 8 o'clock and 11 o'clock positions. Note the opposite ends having a good contact of the matrix with microballoons. Also noticeable are the additional bellow-like features between 4 o'clock and 6 o'clock positions.

1180 kg/m^3. Glass microballoons, Ecospheres SI (supplied by Grace Electronic Materials, Belgium), with a true density of 250 kg/m^3, diameter in the range 44–175 μm for two-phase syntactic foam, were used as closed pore material.

Material processing

Syntactic foams were processed by varying the volume fraction of resin and microballoons, depending upon the desired density. A weighed quantity of resin was heated in a beaker to 95°C. Then a specified quantity of hardener based on the resin-to-hardener ratio mentioned earlier was mixed. At this stage, the weighed quantity of microballoons, in several lots, was added to the system containing resin and hardener, stirring the contents well each time. Gentle mixing was done to avoid the breakage of microballoons until the mix developed as "slurry" for making the two-phase syntactic foams aimed at in this work. The slurry was filled into a metallic mold of dimension 150 mm $\times$ 150 mm $\times$ 25 mm. The mold was then closed and allowed to cure at ambient temperature for 24 h. The cured foam was demolded and post cured, first at 100°C for 4 h followed by another at 160°C for 3 h. Density of the cast slab was found to be 779.5 kg/m^3.

Short beam three point bend tests

Short beam three point bend tests were performed in an INSTRON 8502 microprocessor controlled testing machine. The machine was programmed to apply a load at the rate of 1.3 mm/min. An indigenously designed, fabricated, and previously used fixture[27] aided in applying flexural load to the specimen, which was placed on two roller shaped supports at the ends with enough overhanging of the test coupon as is specified for short beam shear tests. Test samples having dimensions of 3 $\times$ 15 $\times$ 21 mm^3 conforming to 1 : 5 : 7 ratio for thickness : span length : total length, respectively, were used. Four samples were tested in this manner.

As per the objective set out earlier, materials processed the very same way were exclusively tested for uniaxial compression and tension separately, for use as comparison test samples for microscopy.

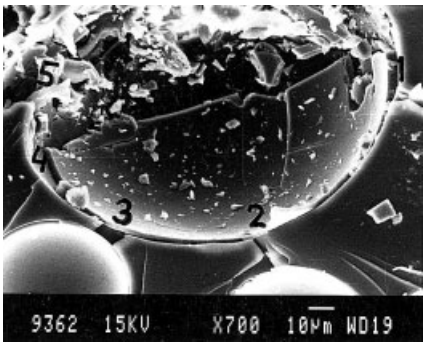

Figure 6 The microballoon showing interface debonding and the emergence of cracks from it at regions marked 1 to 5.

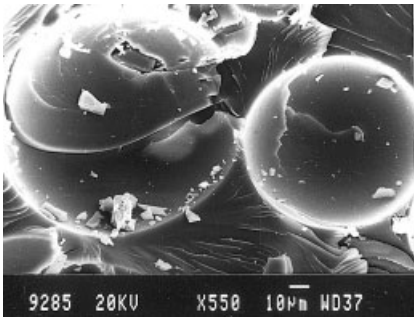

Figure 8 Samples subjected to uniaxial tensile loading showing features of partly developed arctic type crack and the epoxy matrix below showing faintly visible river pattern.

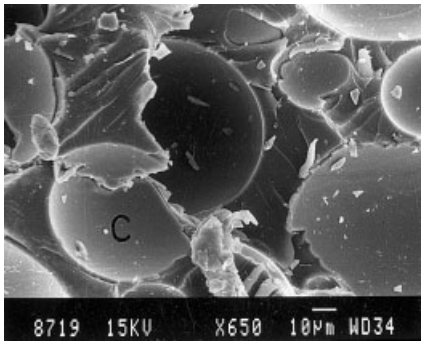

Figure 9 Surface features of uniaxially tensile tested samples showing a partial equatorial crack in the lower center posited microballoon (marked "C").

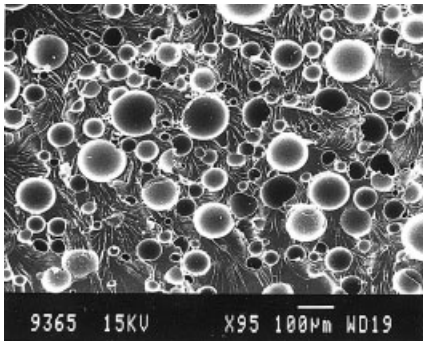

Figure 11 The distribution of microballoons and matrix phases in the mid zone region of the SBT failed sample corresponding to the shear dominated region.

Compression test

Compression tests were performed at room temperature in a DARTEC 9500, a servo-hydraulic, computer controlled testing machine, at a constant strain rate of $0.01s^{-1}$. Specimens having dimension $15 \times 15 \times 7.5$ mm^3 were made for this purpose.[28] The compression-failed samples were examined through a Scanning Electron Microscope (SEM) to note down the features on the failed surfaces.

Tensile test

Tensile tests were performed at room temperature in an MTS 8100, a servo-hydraulic computer controlled testing machine, at a constant cross head speed of 5 mm/min. The dumbbell shaped specimens having a gauge length 25 mm and a total length of 115 mm with a fillet radius of 14 mm and outer radius of 25 mm and conforming to ASTM specification[29] were tested to failure, following which the surfaces of the failed coupons were examined under SEM.

Microscopy

The failed samples from SBT, UC, and UT conditions were examined in a JEOL make JSM 840A SEM to observe the fractographic features. Prior to mounting of the samples in SEM, they were gold coated in a sputtering unit at a current of 10 mA.

RESULTS AND DISCUSSION

As per the objectives set out, the different zones were looked into for their surface features. Thus, Figure 1 shows the tension prevailing end at the top, whereas in the bottom side compressive forces prevail. Figure 2 is the photograph of another sample, in which the specimen, this time, was mounted upside down to that involved in Figure 1. Hence, in this latter case, going by the earlier arguments, the bottom portion of the micrograph shows the tension end of the failed specimen, while the top region shows the compressive forces prevailing zone.

A schematic representation is shown in Figure 3.[30,31] In both Figures 1 and 2, being low magnification pictures, a copious and uniform distribution of microballoons of varying sizes in the epoxy matrix can be seen. To locate the region where the crack could have initiated, a scan of the tension bearing edge was carried out first, and a local region of interest is presented in Figure 4. In this picture, the center as well as the top right corner shows aluminum foil used to position the

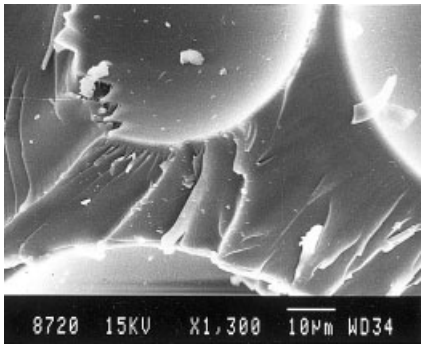

Figure 10 River-like patterns in the matrix phase of uniaxially tension-tested sample.

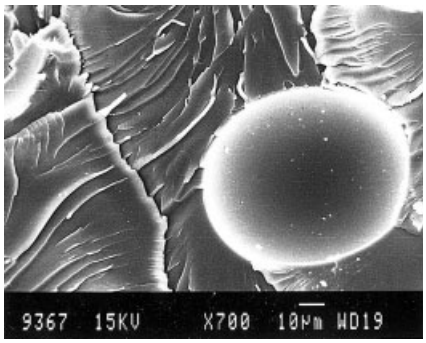

Figure 12 The features around a microballoon highlighting the deformation marks in the matrix.

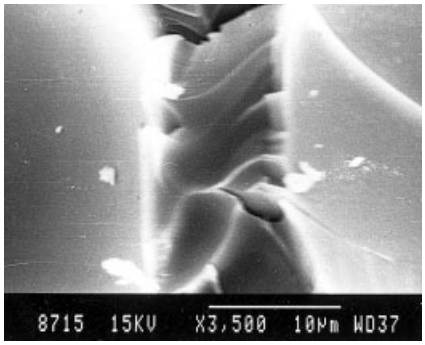

Figure 13 The matrix sandwiched between two microballoons showing extensive deformation and widely open crack at the top and the presence of a smaller one on the lower side of it.

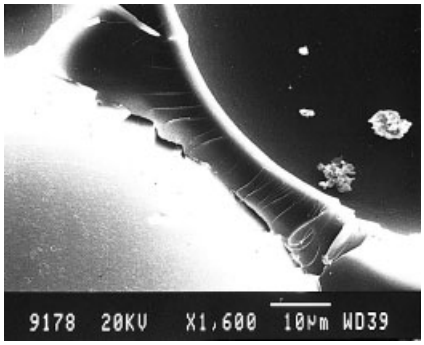

Figure 15 Another sandwiched matrix portion lying between two microballoons where, besides the deformation marks, the part debond with respect to one of the microballoons as well as the debris left on these can be seen.

sample, and a region from where the crack has initiated. Further examination shows that interface separation in some larger microballoons has occurred partly on the periphery of the microballoons (e.g., marked "A" at lower bottom center). When this feature is examined at higher magnification in Figure 5, it shows the interface separation on the top and left part of the microballoons, while the lower bottom and right regions are fairly well bonded to the epoxy resin. A faintly visible equatorial zigzag crack across the microballoon is seen in the left top-most posited (marked "A") bigger-sized microballoon (Fig. 5). This zigzag crack on a comparatively bigger microballoon (marked "B") in the right side of the photograph (Fig. 5) is oriented differently, and it propagates from top to bottom of the microballoon. Incidentally, this microballoon has a partly visible central puncture, underscoring the established fact that microballoons are hollow in nature. Between this and a microballoon at the lower center, a faint river mark (indicated by arrow) can clearly be seen.

To emphasize more on the cracking, on the tension side, a feature of interest in the top face is examined in Figure 6. In this picture the crack originating from the extreme right top portion of the micrograph and propagating through five branches marked 1 to 5 on the circumference of the microballoons, as well as a propagating equatorial crack, can all be clearly seen. The top central part also shows what can be termed "a partially fractured microballoon" due to tensile forces acting in the system. Figure 7 shows the debonding (marked by arrow at "A") of the bigger microballoon in the top and the left side due to tensile forces; while in the bottom and right hand side (marked by arrow at "B") the matrix has undulated/rippled features, indicating that this side of the microballoon experiences a situation that is different from those on its top and left positioned regions.

To correlate these tensile failure patterns, the features derived on a similar sample but subjected to simple uniaxial tension is now considered. Figure 8 shows the failure pattern in tensile loaded situations in which the right hand microballoon shows the partial equatorial crack propagating and developing branches. Figures 9 and 10 show the different regions of this sample that failed in simple tension. Figure 9 shows a crack that during its sojourn produces what may be termed a "partial equatorial crack" in the adjacent microballoon (marked "C"). Figure 10 shows the river-like pattern in the matrix lying among the

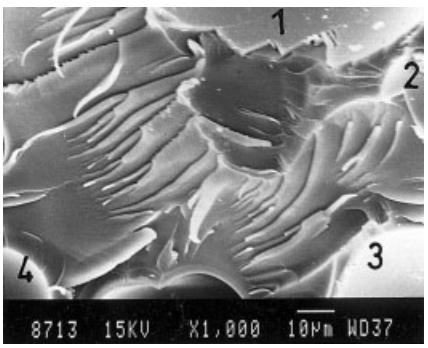

Figure 14 The features of the matrix sandwiched among the four microballoons (marked 1, 2, 3, and 4).

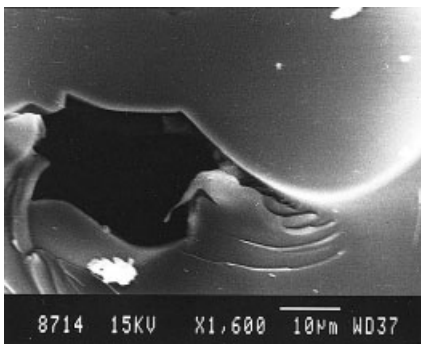

Figure 16 The cavity and the crack spreading into the matrix.

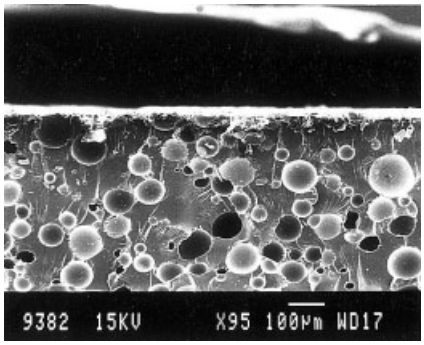

Figure 17 The surface close to the central load application experiencing a compressive deformation. The microballoons dispersed in the matrix are visible.

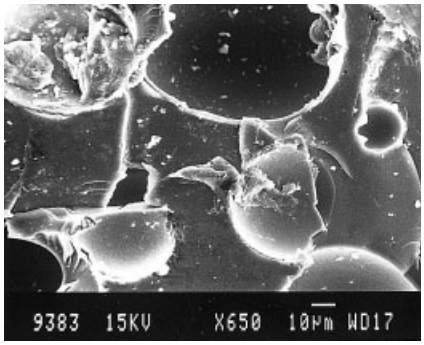

Figure 18 The microballoon in the top left corner showing debris formed from the caving-in phenomenon.

three visible microballoons in the photograph. This clearly shows that the features are typical of a tensile nature. Thus, when the features seen on the outward layer experiencing tension in Figures 5, 6, and 7 are compared with samples subjected to uniaxial tension experiments, displayed in Figures 8, 9, and 10, it is seen that river marks and debonding on one side of the microballoons appear in both cases. This clearly proves that this region, that is, the side away from the loading face, experiences tensile forces. Other minor features seen in Figure 6 are the cracks originating at the tension side, where multiple cracks from the same source appear, indicating that this possibly is the region situated directly under the mid-span loading point.

When the microscopy was done for the region that is midway between the tension and compression sides, the features that resulted are depicted in Figure 11, where the low magnification picture has microballoons of different sizes well dispersed in a matrix of epoxy, which has deformation bands. Figure 12 was taken at a higher magnification, where the deformation bands surrounding a microballoon can clearly be seen. Figure 12 also shows the angularity relationship between the direction of crack propagation and shear banding. To emphasize more on this deformation pattern, these samples were examined at higher magnification, the features of which are presented in Figures 13, 14, 15 and 16. Figure 13 shows the deformation bands in the matrix, which is between the two microballoons, and due to this constrained condition, a partly visible crack is developed in the middle of the matrix and a wider one at the top. Figure 14 shows the shear dominated region of the matrix and the four microballoons. The phenomenon of part debonding is clearly seen in Figure 15. Figure 16 shows the cavity about a microballoon, and the resultant features in the matrix where this cavity leads to the crack initiation process. Thus, the shear mode of deformation for the central (i.e., along fractured thickness) part of the specimen that corresponds to the proximity of the neutral axis in a typical beam experiencing three point bending is clearly brought about in this study.

The topmost portion of the sample, which comes right under the midway situated loading cylinder of the three point bending setup and experiencing compressive loading, obviously has different features. The compression side has the typical features of microballoons crushing and the crushed part being in a sort of "collapsing-in" or "caving-in" mode, as illustrated in Figures 17 and 18. Figure 17, which is the lower magnification of this sample, shows microballoons, coming right under the central cylindrical loading point, have crushed as they are hollow in nature. The other features are the debris in a scattered condition, as evident from Figure 18, where the left top corner has crushed microballoon and the matrix do not readily display the river pattern seen in the matrix-rich region experiencing the tensile forces discussed earlier on. Samples subjected to uniaxial compression tests also show these collapsed microballoon features, as is clear from Figures 19 and 20. Figure 19 shows the crushed microballoon in the central portion and the space inside the hollow microballoons by the collapsing surface filled up by the debris created due to the compression. Thus, there is one to one correlation in both tension and compression zones of the three point

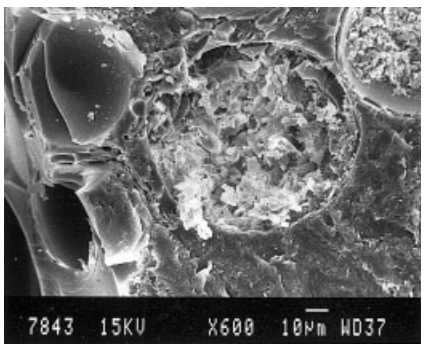

Figure 19 Uniaxial compression sample showing debris in two adjacent microballoons.

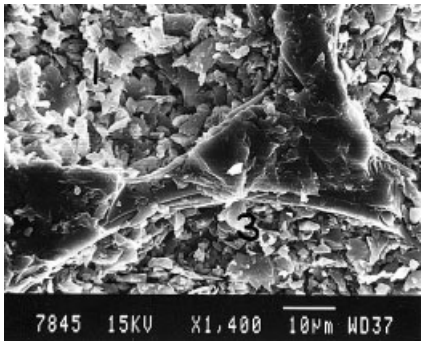

Figure 20 The scattered debris in the uniaxial compressed sample in three (marked 1, 2, and 3) microballoons with epoxy regions sandwiched, showing less of this debris at the central part of the photograph.

bending samples with those seen in uniaxial tension and compression experiments, respectively. The regions about midway between the tension and compression ones show clear deformation features.

CONCLUSIONS

SBT test failed samples examined under microscopy show at one end a predominance of tension bearing forces; while on the other face, compressive bearing ones predominate. The tension dominated face revealed river-like markings, partially fractured microballoons, and interface debonding. When the microscopy was done for a region coming directly below the mid span loading axis of the SBT test, it shows crushing and collapsing of the microballoons' surface, which are hence filled up with debris. Similarly processed syntactic foam samples subjected to a UT test show almost the same fracture features as observed in the tension-dominated region of the SBT test. Similarly, when a sample is subjected to the UC test, it replicates the failure features of the SBT zone, which corresponds to the dominance of compressive forces. This validates that failure features of the tension and compressive zone of the SBT test are similar to those noticed in UT and UC test failed samples, respectively. Hence, failure features observed in syntactic foam depend upon the type of stress state experienced by the system.

When a zone was chosen by avoiding both tension and compression ends of the SBT failed samples, that is, a region midway between the two, it revealed characteristic features of the deformation bands in the matrix-rich region situated between the microballoons.

References

1. Price, H. J.; Nelson, J. B. J Compos Mater 1976, 10, 314.
2. Medhat, A.; El-Hadek, A. M.; Hareesh, V.; Tippur, J. Solid Struct 2003, 40, 1885.
3. Bardelle, L.; Genna, F. Solid Struct 2001, 38, 307.
4. Shutov, F. A. Adv Polym Sci 1986, 73/74, 63.
5. Bunna, P.; Mottram, J. T. Compos 1993, 24, 565.
6. Bardelle, L.; Genna, F. J Solid Struct 2001, 48, 7235.
7. Rizzi, E.; Papa, E.; Corigliano, A. Sci Technol 2000, 60, 2169.
8. Rizzi, E.; Papa, E.; Corigliano, A. Int J Solid Struct 2000, 37, 5773.
9. Kallas, D. H., Chatten, C. K. Ocean Eng 1969, 1, 421.
10. Gupta, N.; Woldesenbet, E. Compos Struct 2003, 61, 311.
11. Ishai, O.; Hiel, C.; Luft, M. Compos 1995, 26, 47.
12. Nikhil, G.; Eyassu, W. Proceedings of the American Society for Composites 17th Technical Conference, Paper 402; Purdue University, West Lafayette, Indiana, October 21–23, 2002.
13. Nikhil, G.; Eyassu, W. Proceedings of SAMPE Symposium, Baltimore, November 4–7, 2002.
14. Kim, H. S.; Plurai, P. Proc ACUN-4, Compos Sys 2002, 21–25 July, 251.
15. Kim, H. S.; Khamis, M. A. Compos 2001, 32, 1311.
16. Karthikeyan, C. S.; Sankaran, S.; Kishore. Polym Int 2000, 49, 158.
17. Jancar, J.; Dibenedetto, A. T. J Mater Sci 1995, 30, 1601.
18. Hussain, M.; Nakahira, A.; Nishijima, S.; Niihara, K. Mater Lett 1996, 27, 21.
19. Hussain, M.; Nakahira, A.; Nishijima, S.; Niihara, K. Mater Lett 1996, 26, 299.
20. Bleach, N. C.; Nazhat, S. N.; Tanner, K. E.; Kellomski, M.; Tormala, P. Biomaterials 2002, 23, 1579.
21. Goyanes, S. N.; Marconi, J. D.; Koing, P. G.; Martin, M. D.; Mondragon, I. J Alloys Compd 2000, 28, 374.
22. Gilchrist, M. D.; Svensson, N. Compos Sci Technol 1995, 55, 195.
23. Steven, W. H.; Chung, D. D. L. Carbon 1995, 33, 1627.
24. Woo, E. M.; Mao K. L. Compos A 1996, 27, 625.
25. Pahr, D. H.; Rammerstorfer, F. G.; Rosenkranz, P.; Humer, K.; Weber, H. W. Compos B 2002, 33, 123.
26. Schneider, K.; Lauke, B.; Beckert, W. Appl Compos Mater 2001, 8, 43.
27. Kishore; Mahajan, S. S.; Kulkarni, S. M. Pract Metallogr 2003, 40, 34.
28. A.S.T.M. D 1621–73, Standard Test Method for Compressive Properties of Rigid Cellular Plastics.
29. A.S.T.M. D 638M-93, Standard Test Method for Tensile Properties of Plastics (Metric).
30. Daniels, B. K.; Harakas, N. K.; Jackson, R. C. Fiber Sci Technol 1971, 3, 187.
31. Popov, E. P. In Mechanics of Materials; Prentice-Hall of India Ltd.: New Delhi, 1965; Chapter 6, p 127.